

Article

A Comparative Analysis of In-Situ Optical Velocimetries for Oil Spill Flow Rate Estimation

Osman Abu Bkar ¹, Mark Ovinis ^{2,*} and Abdalellah O. Mohammed ³

¹ Mechanical Engineering Department, Sudan Technological University, Khartoum 11111, Sudan; anotood@yahoo.com

² Mechanical Engineering Department, Universiti Teknologi PETRONAS, Seri Iskandar 32610, Malaysia

³ School of Engineering, Emirates Aviation University, Dubai, United Arab Emirates; abdalellah@mec.edu.om

* Correspondence: mark_ovinis@utp.edu.my

Abstract: In the Deepwater Horizon oil spill, optical plume velocimetry (OPV), a flow measurement technique for use in seafloor hydrothermal systems, was found to have the least uncertainty in estimating the rate at which oil was escaping from the well in the deep sea. However, OPV still had a high uncertainty of 21%, partly due to the limited accuracy of the temporal cross-correlation algorithm used. In this work, the accuracy of several in-situ optical velocimetries, namely wavelet-based optical velocimetry (WOV), OPV, and two classical correlation-based algorithms, namely fast Fourier transform (FFT) and normalized cross-correlation (NCC), for a plume flow with Reynolds numbers varying from 1847 to 11,656 was investigated. WOVI, FFT, and NCC resulted in flow rates closer to the expected turbulent plume flow rate as compared to OPV. Moreover, a noisy velocity field was found using OPV. The accuracy of wavelet-based algorithm outperformed all cross-correlation based algorithms. The flow rate was measured with an error of 8.5% using WOVI, whereas errors of 18.2%, 19.7%, to 21.1% were obtained when applying FFT, OPV, and NCC, respectively. There was a statistically significant difference between wavelet-based and correlation-based algorithms, but no statistically significant difference between the estimation of the three cross-correlation based velocimetries. WOVI outperformed the other velocimetries and estimated flow rates with an error of 8.5%, whereas the OPV, FFT, and NCC were estimated with errors of 19.7%, 18.2%, and 50.8%, respectively.

Keywords: flow measurement; oil spill; optical technique; cross-correlation



Citation: Bkar, O.A.; Ovinis, M.; Mohammed, A.O. A Comparative Analysis of In-Situ Optical Velocimetries for Oil Spill Flow Rate Estimation. *Fluids* **2022**, *7*, 126. <https://doi.org/10.3390/fluids7040126>

Academic Editor: Giuliano De Stefano

Received: 3 January 2022

Accepted: 14 March 2022

Published: 28 March 2022

Publisher's Note: MDPI stays neutral with regard to jurisdictional claims in published maps and institutional affiliations.



Copyright: © 2022 by the authors. Licensee MDPI, Basel, Switzerland. This article is an open access article distributed under the terms and conditions of the Creative Commons Attribution (CC BY) license (<https://creativecommons.org/licenses/by/4.0/>).

1. Introduction

Optical velocimetry estimates velocity field from image sequence data. Existing techniques can be classified as active, which uses lasers to illuminate the flow space, or passive, which uses external light for illumination. A well-known active technique is particle image velocimetry (PIV) [1]. PIV has many applications in fluid dynamics. PIV measures flow with very high accuracy, more than 99%, for laboratory scale measurements. The good accuracy of PIV in lab-scale applications is in part due to the use of pulsed laser with seed particles, which facilitates particle tracking. However, when PIV was applied to in-situ flow measurement of an oil spill, where no seed particles are present, it underestimated flow rate by a factor of two, with high uncertainty [2]. Techniques such as hot wire velocimetry (HWV) [3,4] and laser doppler velocimetry (LDV) [5] are laboratory-based techniques requiring specialized equipment and calibration and are therefore not appropriate for in-situ applications. In this regard, passive technique such as optical plume velocimetry (OPV) is more appropriate for in-situ applications such as oil spill flow rate estimation from a well blowout.

Regardless of whether an active or passive technique is used, algorithms are required for velocity field estimation from input images. Several algorithms were proposed for the estimation of velocity field from an image sequence. These algorithms can be classified into differential based [6,7], cross-correlation based [8], frequency based [9], and

wavelet-based [10] algorithms. Cross correlation-based methods are widely applied in flow measurement. However, classical algorithms consider only signal amplitude or frequency information, which may not appropriate to deal with turbulent signals. This is because the time resolution of the signal in frequency domain is mostly lost, whereas frequency information is lost in time domain.

To consider both signal amplitude and its frequency in flow estimation, the use of wavelet transform was proposed [11,12]. Tal et al. [13] estimated the time-delay between two non-stationary signals for fluid velocity estimation. Jakubowski et al. [14] and Ching et al. [15] proposed techniques based on wavelet theory for pre-processing and filtering signals prior to velocity determination. Moreover, wavelets has been applied for several applications such as investigation of coherent structure of turbulent flow [16,17], turbulent flow simulation [18], and velocity field estimation [19]. Wavelet theory can deal with non-stationary signals and is therefore an appropriate technique for turbulent flow such as an oil spill jet, at both fine and large scales.

Several researchers have proposed velocimetry for velocity field estimation from an image sequence or video, by combining wavelets with differential based algorithms [20,21]. Good results were obtained for velocity field estimation compared to classical differential-based algorithms, as differential based algorithms alone can be applied only for fine-scale turbulent flow and cannot deal with the large-scale flow such as that of an oil spill. Additionally, by using wavelets, the computational time can be reduced.

Existing wavelet-based velocimetries combine wavelet transform with differential algorithms. These velocimetries have two main problems, including the use of discrete wavelets, which reduce the size of input signals, leading to poor velocity field estimation. Second, the differential algorithm estimates the velocity field based on a fine scale, leading to poor estimation, as oil jets move with high velocity, generating coherent structures that cannot be captured by a differential-based algorithm. Here, the use of discrete wavelet transforms leads to artefact errors, which affect the velocity field. Recently, we developed a novel technique called wavelet-based optical velocimetry (WOV) [6], which is based on wavelet transform and velocity field based on signal amplitude and frequency.

In this work, a comparative analysis of several optical velocimetries to estimate the flow rate of a turbulent plume flow was performed. The next section describes the overall methodology including the experiments tests and velocimetries. Results, discussion, and conclusions follow.

2. Method

To evaluate the optical velocimetries, a turbulent plume flow was experimentally simulated for five flow rates. This section describes the procedure for the experiment, including a description of the experimental apparatus and the video data collection. Additionally, the pre-processing of the input video and the post-processing steps are described in detail. Finally, the performance of the proposed techniques, namely WOV, OPV, FFT, and NCC, are discussed.

2.1. Experimental Apparatus

Figure 1 illustrates the experimental setup used for turbulent plume flow simulation. The set-up includes three tanks: the main tank, a supply tank, and an overhead tank. The main tank is $0.9\text{ m} \times 0.9\text{ m} \times 2\text{ m}$ and is made of acrylic material to allow for recording of the flow outside the tank using a video camera. The large size of the tank prevents a wall effect, in which the flow touches the tank wall. Water with graphite and a 5% salt is used to generate the plume. Salt is added to generate buoyancy to the plume. The overhead tank provides a constant flow rate in the nozzle, as the water level remains constant. A flow control valve is used to control the flow rate. A submersible pump placed in the lower tank replenishes the graphite mixture of the overhead tank. The graphite mixture flows as the control valve is open through an 8-mm diameter nozzle connected from the overhead tank, simulating a plume. A momentum diffuser is used to keep the plume at the bottom of the

main tank. Two underwater 5W LED lights are placed in the main tank to illuminate the flow. A black background is used to improve the visibility of the flow, and a 10×10 mm checker-board pattern is used for calibration purposes.

A Canon EOS-550 camera (Canon, Tokyo, Japan) is used to collect plume flow data for five different flow rates. The camera distance from the nozzle, focal length, focusing level, and field of view were adjusted accordingly. A 120-s video was recorded for each experimental run, at 50 fps frame rate with a resolution of 1280×720 pixels at a standard focal length of 50 mm.

Flow rates were measured to compare the accuracy of velocimetry. By opening the control valve, various plume flow rates were simulated experimentally, and five cases were considered [22]. The control valve was calibrated by recording the time taken for five litres of mixer to flow into the main tank. The five nozzle velocities are 0.18, 0.32, 0.45, 0.62, and 1.16 m/s, with Reynolds numbers ranging from 1847 to 11,656.

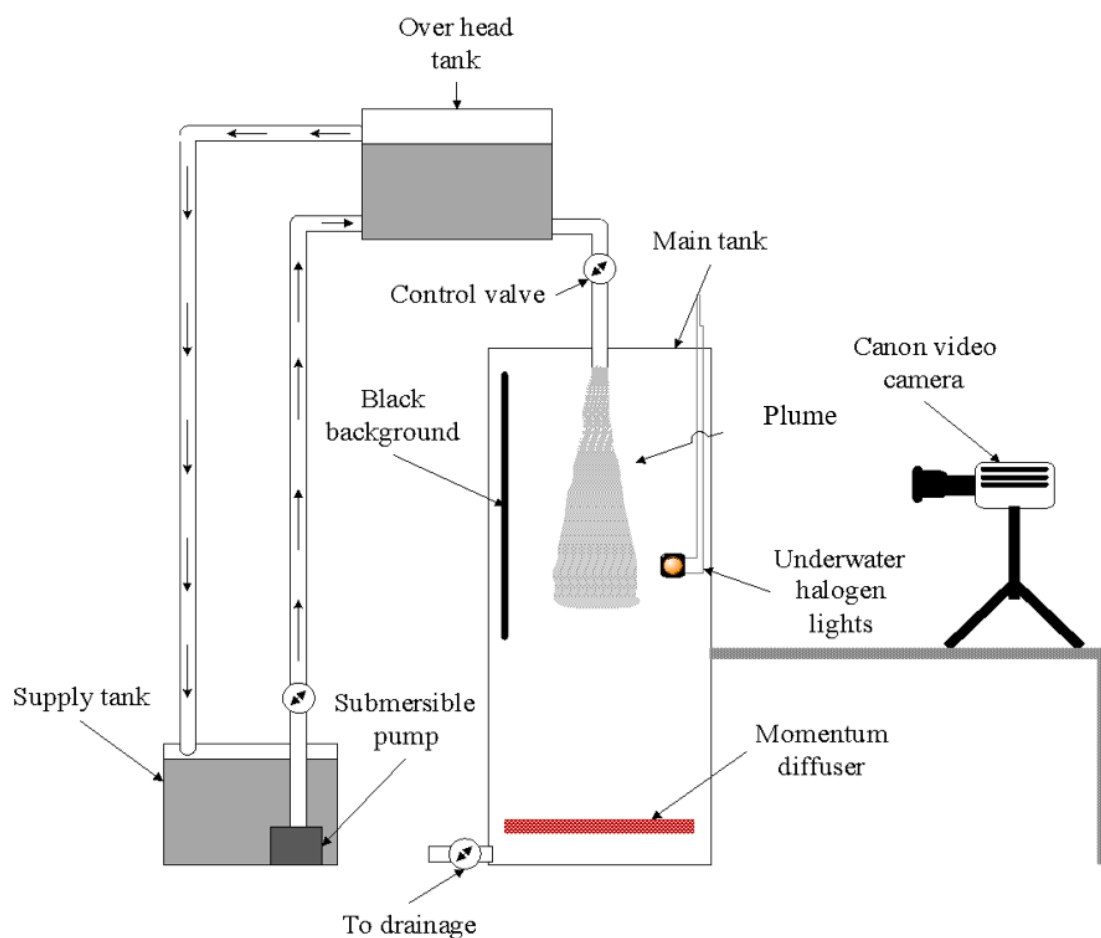


Figure 1. Cont.

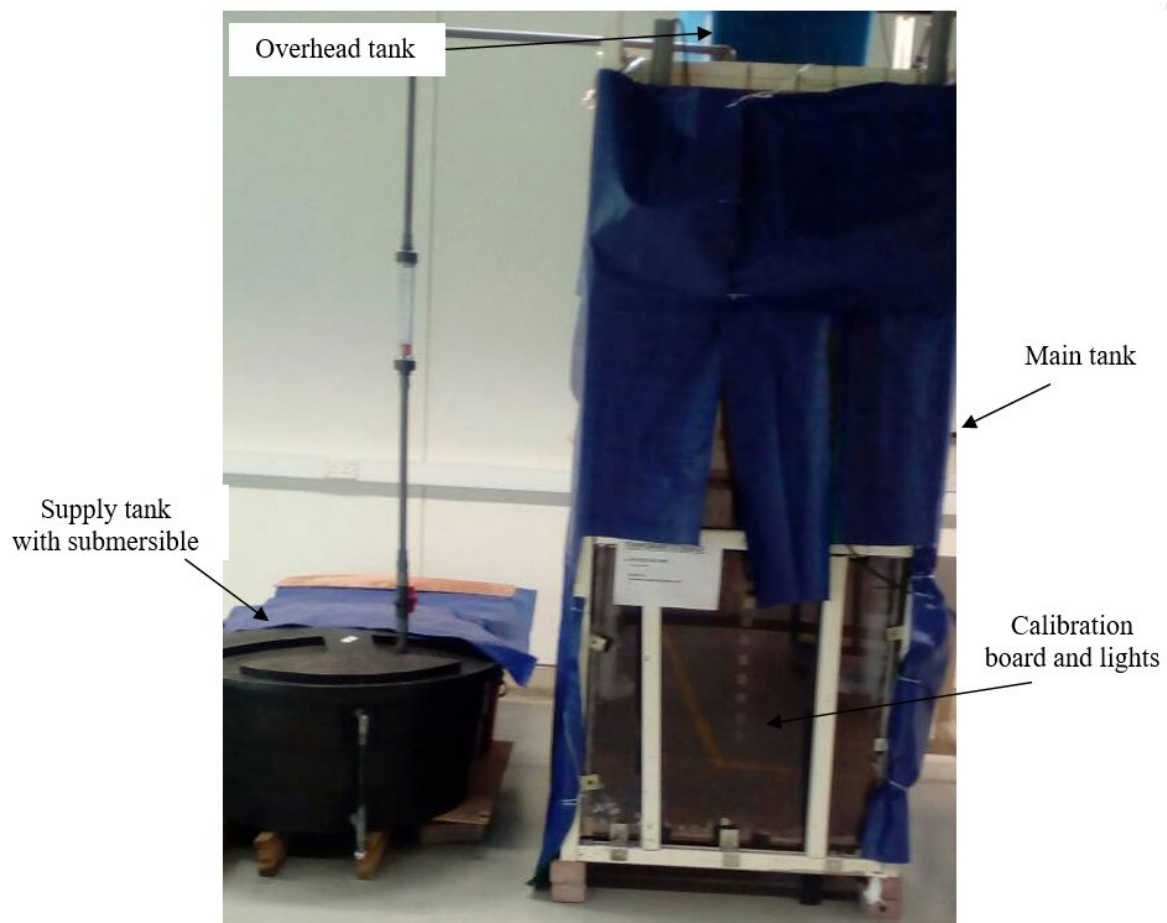


Figure 1. Experimental setup used for plume simulation including schematic (**above**) and actual setup (**below**).

2.2. Pre-Processing of Flow Video

The recorded video was pre-processed to enhance the quality of the output image sequence. The pre-processing steps applied to the video include conversion of the video to an image sequence, conversion of colour images to grayscale, and cropping of the flow region. Image subtraction was applied to all images to remove the background. Next, the contrast of the input images was enhanced using adaptive histogram equalization. Figure 2 shows a sample of the original frame extracted from a video of the flow for the first flow rate, the image after background subtraction, and the enhanced image. The processed image appears smoother than the original image, in which background subtraction removed shadows around the flow, mostly around the plume boundary.

Post-processing was subsequently applied to the image velocity field prior to flow rate estimation. A median filter was applied to remove outliers of the final velocity field. A median filter [5] was applied to the output velocity, and all outliers were replaced by the median of velocities at a defined window with size of 5×5 pixels. Additionally, convolution was performed using a window with size of 5×5 pixels to smooth the final velocity field. By averaging the velocities at the near-nozzle region, the plume velocity was obtained.

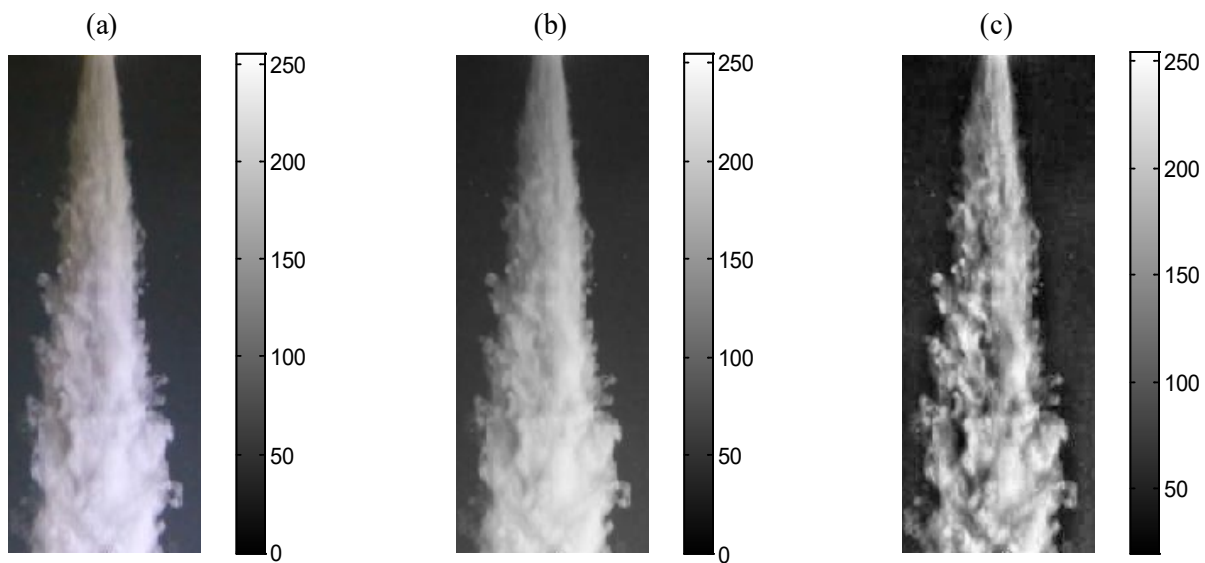


Figure 2. A sample of the (a) original image, (b) image after background subtraction, and (c) enhanced image using adaptive histogram equalization.

2.3. Optical Velocimetries

Four optical velocimetries—WOV, OPV, FFT, and NCC—were applied for image velocity field and flow rate estimation. In all cases, the local velocity was found from a set of image sequences by finding the correlation between two signals extracted from flow space. For two points separated by distance d , with a time-lag t , the velocity at the point, u using Equation (1) is:

$$u = \frac{d}{t} \quad (1)$$

A separation distance of 5 pixels [22] was chosen to extract the signals and estimate the image velocity field. The flow rate was then estimated from the image velocity field by segmenting the image velocity using the Otsu thresholding method [23] by defining a threshold value between the flow and the image background, with pixels below the threshold value removed. This method was applied by Crone et al. [22] as well, for segmenting the image velocity field. The flow rate was then estimated from the velocity field for the four algorithms. Several averaging approaches can be used to estimate the flow rate from the image velocity field, including averaging of the overall velocity field, averaging a certain region from the velocity field, or by defining a threshold to reject some velocity vectors and averaging the remaining vectors. Selection of an averaging approach is an important factor for correlating the estimated flow rate to the actual flow rate. In this work, the flow rate was obtained by averaging the velocity field at a distance equal to the nozzle diameter, i.e., $x/d = 1$, where x is axial distance and d is nozzle diameter, as the flow rate near the nozzle region is closer to the actual flow rate. A linear relationship with zero crossing is expected for the estimated flow rate and the actual flow rate [22].

2.3.1. Wavelet-Based Optical Velocimetry

Four steps are required to estimate flow rate when applying WOVS. The first is the extraction of two signals from flow space over time, with a pre-defined separation distance between those signals. Second, by using continuous wavelet transform, the input signal is transformed to the wavelet domain, which generates wavelet coefficients. In this step, wavelet parameters such as wavelet function, wavelet scales, and vanishing moment are important considerations. The similarity between the wavelet coefficients of the two signals is subsequently determined. By using fast Fourier transform, the peak position of the time-lag between signals, from which velocity can be estimated, can be found. By repeating these steps, the overall velocity field can be obtained by shifting to other points in the image

space. Finally, the flow rate can be obtained by averaging the velocity field. More details on WOV technique can be found in [6], which describes the methodology of image velocity field estimation by WOV.

2.3.2. Optical Plume Velocimetry

Optical Plume Velocimetry (OPV) uses a temporal cross-correlation (TCC) algorithm for image velocity field estimation. TCC is based on the similarity measure between signals or images. TCC was applied by Crone et al. [22] for his OPV technique to determine flow rate from images. The corresponding correlation coefficient R_{TCC} , given by Equation (2) is:

$$R_{TCC}(d) = \sum_{k=1}^{N-1} a_{id,j,k} \cdot a_{i,j,k+l} \tag{2}$$

The summation of the multiplication of the two signals will result in correlation coefficients for a given time lag. The value of time lag, l_{TCC} , can be determined by detecting the maximum correlation coefficients R_{TCC} , using Equation (3):

$$l_{TCC} = \arg_t \max[R_{TCC}(\tau)] \tag{3}$$

2.3.3. Normalized Cross Correlation

The third velocimetry is based on normalizing the turbulent signals prior to cross correlation. This algorithm is called normalized cross-correlation (NCC), which is useful for better correlation and peak detection. A similar algorithm has been applied for estimating the velocity field using the PIV technique [24]. However, in the work of Thomas [24], the cross correlation was implemented in a 2D space, whereas in this work, the NCC algorithm was utilized to find the correlation between each signal for 1D signals. If the input signal is $w(a,b)$, then each scale can be normalized by using Equation (4):

$$\bar{w}^n(a, b) = \frac{w(a, b) - \bar{w}(a, b)}{\|w(a, b) - \bar{w}(a, b)\|_2} \tag{4}$$

where $\bar{w}^n(a, b)$ are the normalized coefficients at scale a , and $\bar{w}(a, b)$ is the mean of correlation coefficients.

2.3.4. FFT Cross-Correlation

The second function considered for time-lag estimation is the FFT cross-correlation, which measures the similarity between two signals in the frequency domain. The FFT algorithm was used to estimate the correlation coefficients between two signals. If the two signals are delayed by a time lag, this lag can be estimated using the FFT to determine the time lag between two signals in three steps: finding the Fourier transform of the two signals, multiplying them together, and finding the inverse FFT of the multiplication to give the required correlation coefficients. The FFT function is given by Equation (5):

$$R_{FFT} = FFT(S_2) \cdot * IFFT(S_1) \tag{5}$$

where S_1, S_2 are the original and delayed signals, respectively.

To find FFT of a signal of $f(n)$ that has a length of n , the following equation is used:

$$F(x) = \sum_{n=0}^{N-1} f(n) e^{-j2\pi(\frac{n}{N}x)} \tag{6}$$

and the inverse FFT is given by:

$$f(n) = \sum_{n=0}^{N-1} F(x) e^{-j2\pi(\frac{n}{N}x)} \tag{7}$$

where $F(x)$ is the frequency domain signal.

Once correlation coefficients are estimated, the required time lag l_{FFT} can be obtained by detecting the maximum of these coefficients, as given by Equation (8):

$$l_{FFT} = \arg_t \max[R_{FFT}(\tau)] \quad (8)$$

3. Results and Discussion

The robustness of the WOV, OPV, FFT, and NCC optical velocimetry methods were subsequently evaluated. These velocimetry methods were applied to estimate the velocity field of plume flow from image sequences for the five nozzle velocities. Figure 3 shows a sample of the velocity field obtained based on the different algorithms. The colour of the estimated velocity field was adjusted between zero to the actual nozzle velocity. From the flow visualization, almost similar velocity fields were obtained when using WOV, OPV, and FFT algorithms. The NCC algorithm underestimated the velocity field and a noisy velocity field resulted. The empty velocity region by NCC was due to infinite velocity magnitudes by the algorithm, which was filled by zeros. A quantitative evaluation shows that both velocity fields obtained by WOV and OPV were more acceptable compared to the FFT and NCC algorithms (see Figure 3). Maximum velocity was obtained in the near-field region, with the velocity gradually decaying away from the nozzle, as predicted from the theory of turbulent jet. The velocity fields obtained using the WOV, OPV, and FFT algorithms are consistent with the predictions of jet theory, in which high velocity is observed in the near-nozzle region, with comparable velocity distribution. However, a quantitative evaluation is required to differentiate between the accuracy of these algorithms.

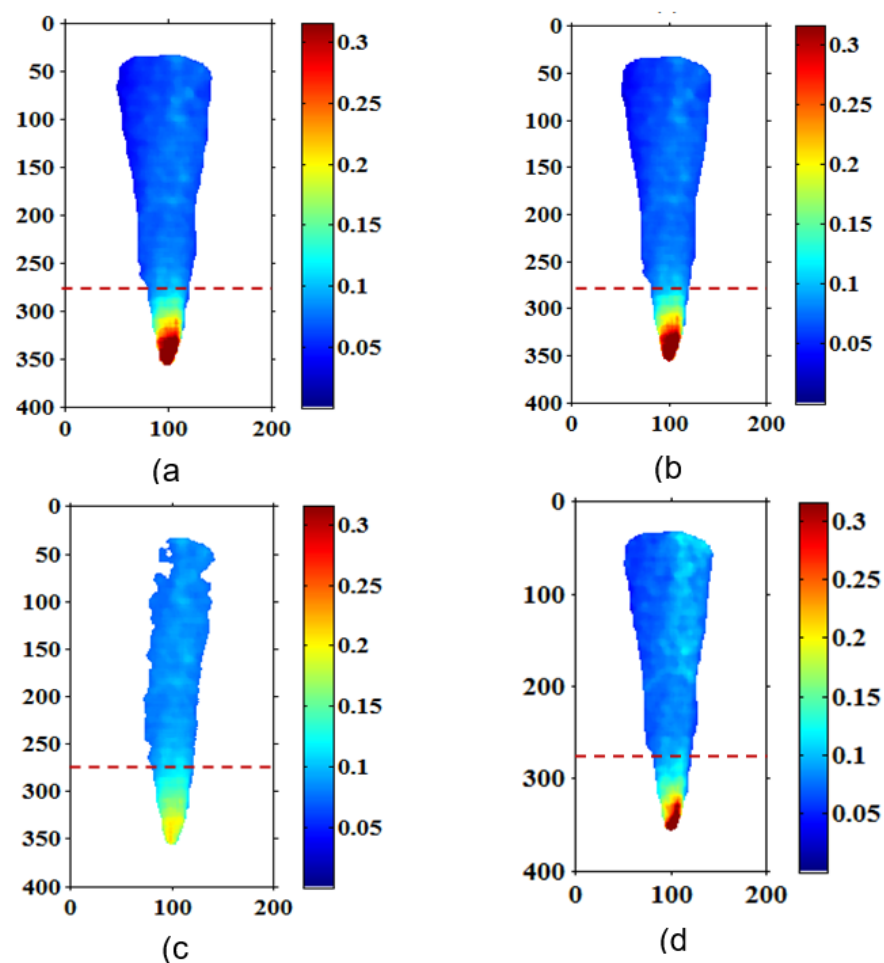


Figure 3. Comparison of image velocity field estimated using (a) WOV, (b) OPV, (c) NCC, and (d) FFT based velocimetry methods.

The estimated velocity field was analysed by extracting the centreline velocity and the radial velocity at three locations in the fully developed region of the simulated jet. Turbulent jet flow theory suggests self-similarity of the radial velocity of different locations in the fully developed region, with a Gaussian distribution.

Figure 4 shows the decays of centreline velocity extracted from the velocity field, obtained by the wavelet-based technique. The growth rates of centreline velocity were 3.3, 3.4, 4.5, 4.7, and 4.8 for the different nozzle flow rates. The wavelet-based technique was able to differentiate different nozzle flow rates, as the nozzle flow rate and jet growth rate increased. However, the growth rates were lower than the predicted growth rate. Lipari et al. [25] found that the range of growth rates for free turbulent jet flow to be between 5.7 to 6.7 for higher nozzle flow rate, compared to the range of flow rate considered in this study. The growth rate range is acceptable, as the maximum flow rate has a Reynold number of 11,656, whereas those reported in the literature were for higher flow rates.

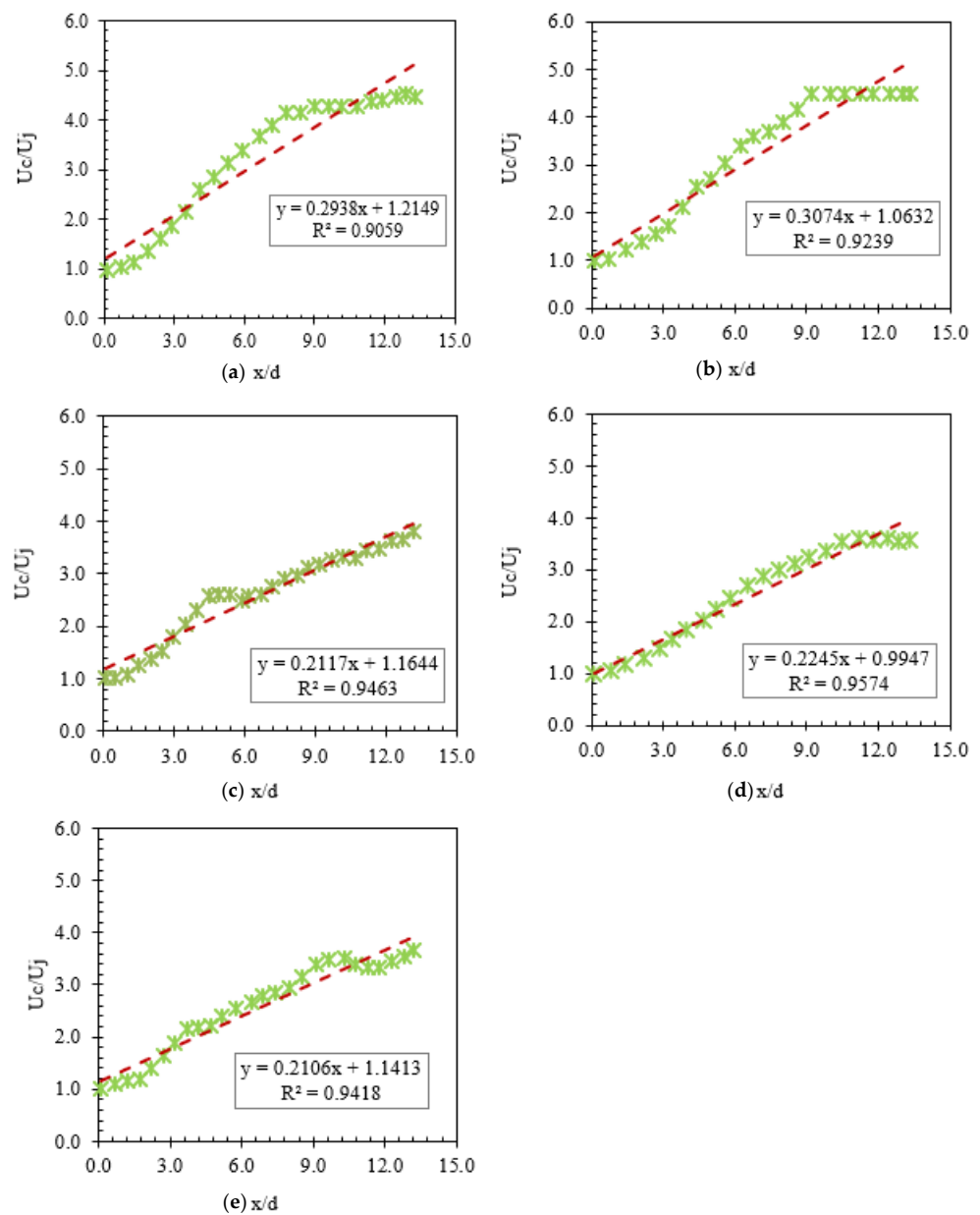


Figure 4. Decay of centreline velocity for nozzle velocity at (a) 0.18 m/s, (b) 0.32 m/s, (c) 0.45 m/s, (d) 0.62 m/s, and (e) 1.16 m/s.

Radial velocities at three locations were extracted from the velocity field estimated by the wavelet-based technique. The normalization of these radial velocities with its maximum usually results in Gaussian profiles. Figure 5 shows the normalized radial velocity at three locations selected at the fully developed region, i.e., $x/d > 6$ including $x/d = 15, 20,$ and 25 . The normalization of the velocity distribution at different locations by the centreline velocity should exhibit self-similarity, in which a Gaussian distribution is predicted. All the radial velocities extracted from the velocity field obtained by the wavelet-based technique are in a good agreement with the predicted Gaussian profiles. The velocity distributions have similar trends with small differences, as compared to the Gaussian profiles. Moreover, the peak positions of theoretical radial velocity were seen at the centre, whereas for the estimated profiles it deviated either to the left or right. This is acceptable as there are some uncertainties in velocity field estimation associated with the experiments and input image sequence.

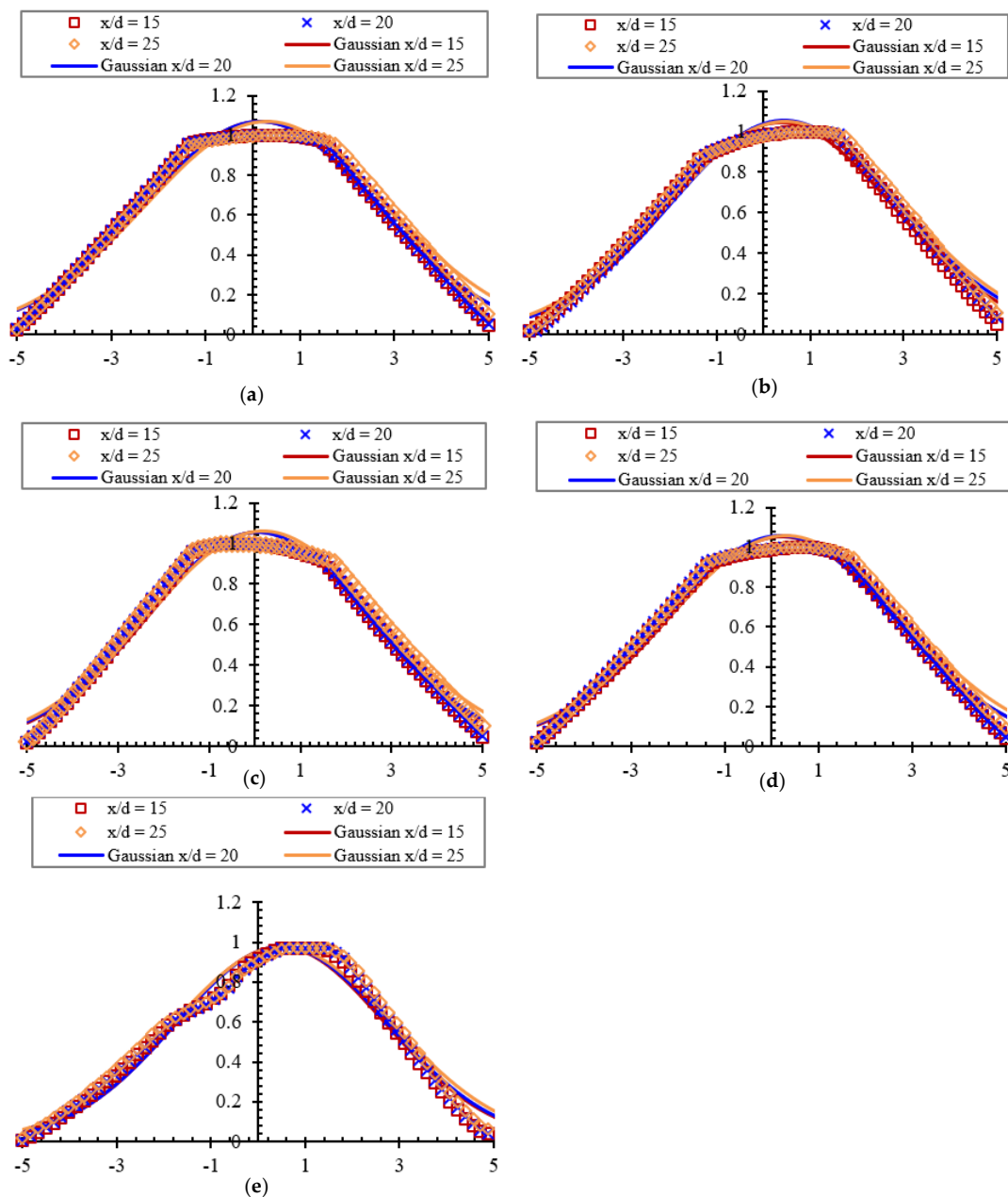


Figure 5. Radial velocity at various axial distances for different nozzle velocity: (a) 0.18 m/s, (b) 0.32 m/s, (c) 0.45 m/s, (d) 0.62 m/s, and (e) 1.16 m/s.

One way to evaluate the accuracy of these algorithms is by testing the linearity response in nozzle velocity estimation and by calculating the error between estimated and the experimental nozzle velocity. For WOV, OPV, FFT, and NCC, the nozzle velocity was estimated as the average of velocities at the near-nozzle region, i.e., under the dash-lines in Figure 3. Figure 6 shows the linear relationship between the estimated nozzle velocity, U_p and the experimental nozzle velocity, W_p . A linear relationship between the estimated and experimental nozzle velocity was obtained for all algorithms. Both OPV and FFT have almost similar trends and are closer to the experimental trend compared to the result of NCC. For the NCC, the estimated velocities were far from the experimental magnitudes, with the nozzle velocity estimated using WOV algorithm closer to the experimental trend. Comparison of linearity response for the estimated nozzle velocity showed that the WOV estimated with non-zero crossing of -0.16 , whereas the non-zero crossing for the OPV, FFT, and NCC algorithms were -0.14 , -0.13 , and -0.31 , respectively.

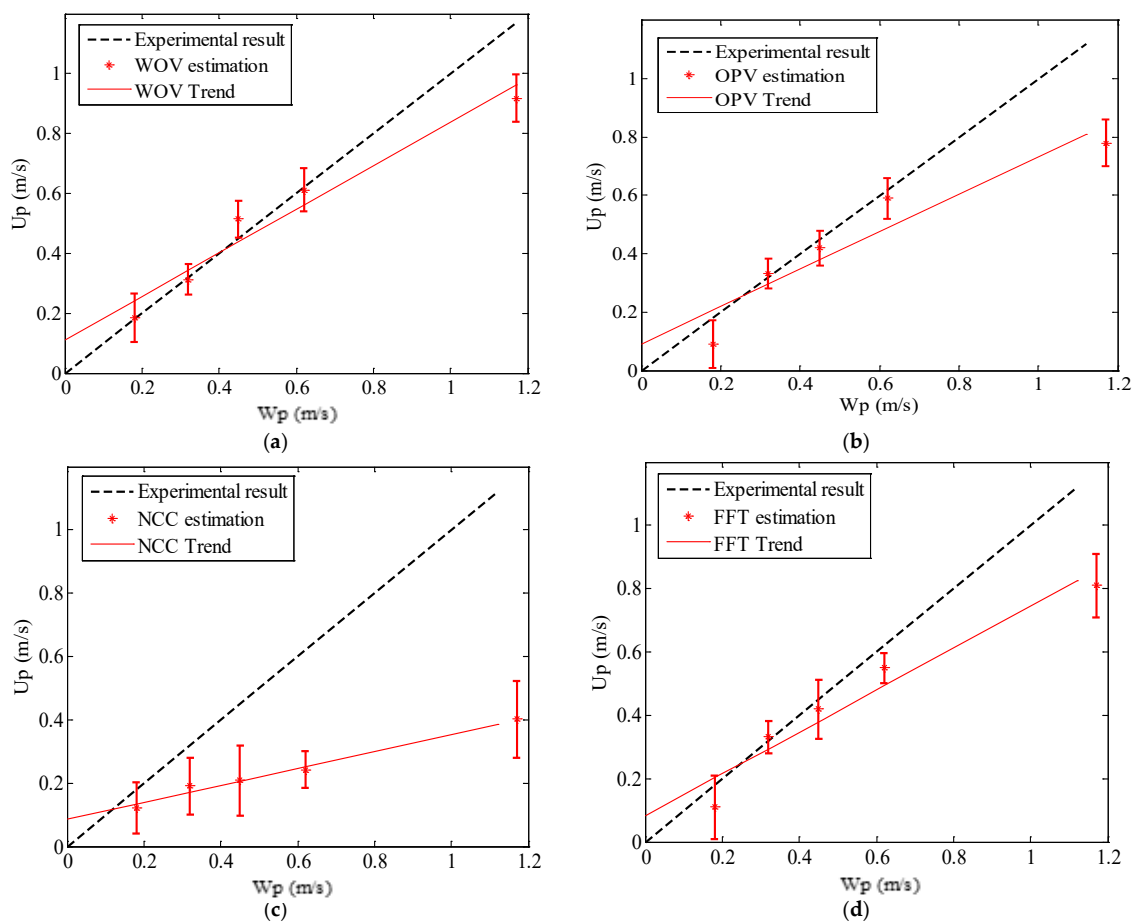


Figure 6. Estimated nozzle velocity compared to the measured velocity for (a) OPV. (b) FFT. (c) normalized FFT. and (d) WOV velocimetries.

Figure 7 shows a comparison of the mean absolute percentage error calculated between the estimated nozzle velocity and the actual velocity for the different optical velocimetries. The WOV technique was found to outperform the other techniques with the estimated the nozzle velocity having an error of 8.5%, whereas the OPV, FFT, and NCC algorithms estimated the nozzle velocity with errors of 19.7%, 18.2%, and 50.8%, respectively. WOV outperformed the classical optical velocimetries and is 56.9% more accurate compared to OPV. WOV enables better correlation between turbulent signals and accurate detection of the time lag between flow signals, from which the velocity is estimated. This is due to the property of wavelet transform in decomposing turbulent signals into multi-scale, which is well suited for turbulent motion. Moreover, WOV has the advantage of considering

time-frequency information, whereas the other velocimetries estimates the velocity either in the time domain or the frequency domain.

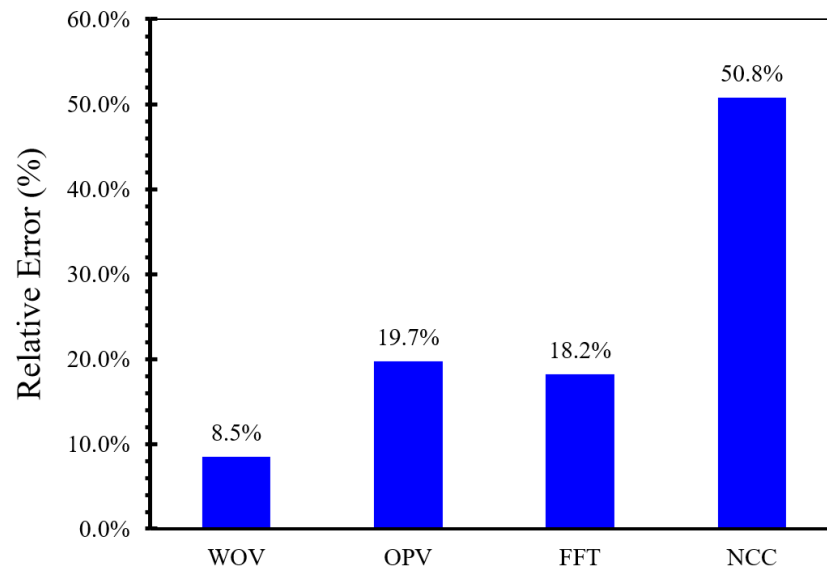


Figure 7. Comparison between in-situ optical velocimetries.

Table 1 shows the accuracy of OPV, FFT, NCC, and WOV, in which the experimental flow rate, U_p is compared with the estimated flow rate, W_p . The flow rates for case 1 and case 2 were measured with high uncertainties, where the error ranged from 30.7% to 50% because of the correlation distance. Selection of correlation distance was based on the need for a large time lag between the two signals, with a larger time lag providing higher measurement accuracy [1]. However, a larger time lag reduces the correlation between the signals. Too small a correlation distance leads to small time-lag values, which makes it difficult to determine its correct value, affecting the accuracy of the algorithm for velocity field estimation. The flow rates for case 2, case 3, and case 4 were measured with acceptable uncertainties, where the error ranged from 3.5% to 15.6%. The better measurement in these cases is because of the correlation distance. The overall accuracy of the three cross-correlation functions was evaluated by taking the mean average percentage error, MAPE, as a reference. WOV outperformed other velocimetries and estimated with an error of 8.5%. However, there was no significant difference between the accuracy of FFT and OPV, whereas the worst results were obtained when using NCC.

Table 1. Comparison between the optical velocimetries (OPV, FFT, NCC, WOV).

No.	U_p (m/s)	Optical Velocimetry							
		OPV		FFT		NCC		WOV	
		W_p (m/s)	RE (%)	W_p (m/s)	RE (%)	W_p (m/s)	RE (%)	W_p (m/s)	RE (%)
1	0.18	0.09	50	0.11	38.9	0.12	33.3	0.19	3.5
2	0.32	0.3311	3.5	0.3311	3.5	0.291	9.1	0.31	2.2
3	0.45	0.4195	6.8	0.4195	6.8	0.381	15.3	0.51	14.3
4	0.62	0.59	4.8	0.55	11.3	0.523	15.6	0.61	1.3
5	1.16	0.78	33.3	0.8105	30.7	0.795	32.1	0.92	21.6
-	-	MAPE	19.7	MAPE	18.2	MAPE	50.8	MAPE	8.5

4. Conclusions

Several optical velocimetries were applied for flow rate estimation. A plume was simulated experimentally by collecting video recordings for five different flow rates with Reynolds numbers ranging from 1847 to 11,656. WOV showed a better estimation than other velocimetries. It outperformed OPV, where the flow rate was measured with an error of 8.5% using WOV and 19.7% for OPV. WOV has the advantage of signal scaling prior to the correlation step, which leads to improved accuracy.

Author Contributions: Conceptualization, M.O.; methodology, M.O., O.A.B. and A.O.M.; software, O.A.B.; validation, O.A.B.; formal analysis, O.A.B.; investigation, O.A.B.; resources, M.O. and O.A.B.; data curation, O.A.B.; writing—original draft preparation, O.A.B.; writing—review and editing, M.O., O.A.B. and A.O.M.; visualization, O.A.B.; supervision, M.O.; project administration, M.O.; funding acquisition, M.O. All authors have read and agreed to the published version of the manuscript.

Funding: This research was funded by Yayasan Universiti Teknologi PETRONAS grant number 015LC0-180.

Acknowledgments: The authors would like to express their appreciation to Universiti Teknologi PETRONAS for supporting this work under YUTP 015LC0-180.

Conflicts of Interest: The authors declare no conflict of interests.

References

1. Westerweel, J.; Elsinga, G.E.; Adrian, R.J. Particle Image Velocimetry for Complex and Turbulent Flows. *Annu. Rev. Fluid Mech.* **2013**, *45*, 409–436. [\[CrossRef\]](#)
2. Lehr, B.; Aliseda, A.; Bommer, P.; Espina, P.; Flores, O.; Lasheras, J.; Leifer, I.; Possolo, A.; Riley, J.; Savas, O.; et al. *Deepwater Horizon Release Estimate of Rate by PIV*; Report to the US Dept of Interior; Flow Research Technology Group (FRTG): Washington, DC, USA, 2010.
3. Heskestad, G. Hot-Wire Measurements in a Plane Turbulent Jet. *J. Appl. Mech.* **1965**, *32*, 721–734. [\[CrossRef\]](#)
4. Ikeda, T.; Fuse, R.; Hatanaka, K.; Hirota, M.; Saito, T.; Rao, S. Investigations on Compressible Mixing Layers by Using Hot-Wire Velocimetry. In Proceedings of the 31st International Symposium on Shock Waves 1, Nagoya, Japan, 9–14 July 2019; pp. 1217–1224.
5. Wang, H.; Lee, S.; Hassan, Y.A.; Ruggles, A.E. Laser-Doppler measurements of the turbulent mixing of two rectangular water jets impinging on a stationary pool. *Int. J. Heat Mass Transf.* **2016**, *92*, 206–227. [\[CrossRef\]](#)
6. Chen, X.; Zillé, P.; Shao, L.; Corpetti, T. Optical flow for incompressible turbulence motion estimation. *Exp. Fluids* **2015**, *56*, 1–14. [\[CrossRef\]](#)
7. Osman, A.B.; Ovinis, M.; Osei, H.; Hashim, F.M. A Review of Optical Flow Models Applied for Fluid Motion Estimation. *ARNP J. Eng. Appl. Sci.* **2016**, *11*, 12181–12187.
8. Beck, M.S.; Płaskowski, A. *Cross Correlation Flowmeters, Their Design and Application*; CRC Press: Boca Raton, FL, USA, 1987.
9. Luo, J.; Konofagou, E.E. A fast normalized cross-correlation calculation method for motion estimation. *IEEE Trans. Ultrason. Ferroelectr. Freq. Control* **2010**, *57*, 1347–1357. [\[CrossRef\]](#) [\[PubMed\]](#)
10. Osman, A.; Ovinis, M.; Hashim, F.; Faye, I. Wavelet-based optical velocimetry for oil spill flow rate estimation. *Measurement* **2019**, *138*, 485–496. [\[CrossRef\]](#)
11. Farge, M. Wavelet transforms and their applications to turbulence. *Annu. Rev. Fluid Mech.* **1992**, *24*, 395–458. [\[CrossRef\]](#)
12. Borgnat, P. *Turbulence and Signal Analysis*; Pennsylvania State University: State College, PA, USA, 2005.
13. Tal, B.; Bencze, A.; Zoletnik, S.; Veres, G.; Por, G. Cross-correlation based time delay estimation for turbulent flow velocity measurements: Statistical considerations. *Phys. Plasmas* **2011**, *18*, 122304. [\[CrossRef\]](#)
14. Jakubowski, M.; Fonck, R.J.; Fenzi, C.; McKee, G.R. Wavelet-based time-delay estimation for time-resolved turbulent flow analysis. *Rev. Sci. Instrum.* **2001**, *72*, 996–999. [\[CrossRef\]](#)
15. Ching, P.; So, H.; Wu, S. On wavelet denoising and its applications to time delay estimation. *IEEE Trans. Signal Process.* **1999**, *47*, 2879–2882. [\[CrossRef\]](#)
16. Shaw, P.K.; Saha, D.; Ghosh, S.; Janaki, M.; Iyengar, A.S. Investigation of coherent modes in the chaotic time series using empirical mode decomposition and discrete wavelet transform analysis. *Chaos Solitons Fractals* **2015**, *78*, 285–296. [\[CrossRef\]](#)
17. Camussi, R. Coherent structure identification from wavelet analysis of particle image velocimetry data. *Exp. Fluids* **2002**, *32*, 76–86. [\[CrossRef\]](#)
18. Magarey, J.; Kingsbury, N. Motion estimation using a complex-valued wavelet transform. *IEEE Trans. Signal Process.* **1998**, *46*, 1069–1084. [\[CrossRef\]](#)
19. Farge, M.; Kevlahan, N.; Perrier, V.; Goirand, E. Wavelets and turbulence. *Proc. IEEE* **1996**, *84*, 639–669. [\[CrossRef\]](#)
20. Dérian, P.; Héas, P.; Herzet, C.; Mémin, E. Wavelet-based fluid motion estimation. In *Scale Space and Variational Methods in Computer Vision*; Springer: Cham, Switzerland, 2012; pp. 737–748.

21. Benezeth, Y.; Jodoin, P.M.; Emile, B.; Laurent, H.; Rosenberger, C. Comparative study of background subtraction algorithms. *J. Electron. Imaging* **2010**, *19*, 033003. [[CrossRef](#)]
22. Crone, T.J.; McDuff, R.E.; Wilcock, W.S.D. Optical plume velocimetry: A new flow measurement technique for use in seafloor hydrothermal systems. *Exp. Fluids* **2008**, *45*, 899–915. [[CrossRef](#)]
23. Otsu, N. A threshold selection method from gray-level histograms. *Automatica* **1975**, *11*, 285–296. [[CrossRef](#)]
24. Thomas, M.; Misra, S.; Kambhamettu, C.; Kirby, J.T. A robust motion estimation algorithm for PIV. *Meas. Sci. Technol.* **2005**, *16*, 865–877. [[CrossRef](#)]
25. Lipari, G.; Stansby, P.K. Review of Experimental Data on Incompressible Turbulent Round Jets. *Flow Turbul. Combust.* **2011**, *87*, 79–114. [[CrossRef](#)]